Structures 14 (2018) 15–31

Contents lists available at ScienceDirect

Structures

journal homepage: www.elsevier.com/locate/structures

Resistance of Axially Loaded T- and X-Joints of Elliptical Hollow Sections at Elevated Temperatures – A Finite Element Study

E. Ozyurt[a], Y.C. Wang[b,*]

[a] Department of Civil Engineering, Gumushane University, Gumushane, Turkey
[b] School of Mechanical, Aerospace and Civil Engineering, University of Manchester, UK

ARTICLE INFO

Keywords:
Elliptical Hollow Section (EHS)
Finite element (FE)
T-joints
X-joints
Static strength
Elevated temperatures

ABSTRACT

This study presents the results of a numerical study to develop a method to calculate the static strength of welded Elliptical Hollow Section (EHS) joints at elevated temperatures. Extensive numerical simulations using the non-linear finite element package, ABAQUS v6.14–1 on EHS T- and X-joints under brace axial compression or tension and pre-stress in chord member with different type of joint orientations at elevated temperatures over a wide range of diameter ratio have been conducted. The adjustments required to be made to the equations of joint resistance under ambient temperature conditions for estimating joint resistance at elevated temperature conditions are investigated in this study. The FE simulation results have been compared with the calculation results of a number of existing methods at ambient temperature. It has been found that the method proposed by Packer et al. gives the best agreement with the authors' simulation results at ambient temperature. At elevated temperatures, for T- and X- joints with braces in compression welded to the wide sides of chords, replacing the ambient temperature yield strength of steel by the elevated temperature value in the current design method overestimates the ultimate load carrying capacity of axially loaded EHS T- and X-joints due to inability of the ambient temperature calculation equations to take into consideration EHS flattening at high temperatures. For these cases, it is recommended to calculate the joint strength reduction factor at elevated temperatures according to the Young's modulus of steel.

1. Introduction

Elliptical Hollow Sections (EHSs) have recently become more popular for architectural applications due to their favourable aesthetics and elegant appearance. EHSs have advantages compared to circular hollow sections (CHSs) and rectangular hollow sections (RHSs). From the architectural point of view, EHSs give a sense of slenderness since their minor diameter is half the major diameter and these sections do not have distinct edges like RHSs. Therefore, EHSs allow us to build aesthetically pleasing structures. In terms of engineering standpoint, EHSs have higher flexural and torsional resistance and decrease wind loading effect due to smooth curvature [1–3]. Applications of these steel profiles include bridges, airports, exhibition halls, etc. (see Fig. 1). This study focuses on elevated temperature resistance of joints which are generally the most critical part of the structure. The authors have previously investigated elevated temperature resistance of welded SHS and CHS joints [4] and this research extends the study to EHS joints.

Compared to the research existing on the welded CHS and RHS joints, there is a paucity of research on EHS joints at either ambient or elevated temperatures. Bortolotti et al. [5] and Pietrapertosa et al. [6] conducted a number of tests on EHS X- and N-joints at ambient temperature, however the tests were terminated before joint failure was reached due to a lack of capacity of the loading jack. Choo et al. [7] numerically modelled EHS X joints to examine the behaviour in various orientations as shown in Fig. 2. They concluded that the joint capacity decreased from type 4, 3, 2 to 1. Shen et al. [8–11], Wardenier et al. [12] and Packer et al. [13] investigated EHS X-joints with braces welded to either the narrow or wide side of the chord when the braces

* Corresponding author.
E-mail address: yong.wang@manchester.ac.uk (Y.C. Wang).

https://doi.org/10.1016/j.istruc.2018.01.004
Received 15 August 2017; Received in revised form 25 January 2018; Accepted 27 January 2018
Available online 31 January 2018

Notations

A_{chord}	Cross sectional area of chord member
B	Smaller diameter of chord member
C_1	Constant
D	Larger dimension of chord member
L	Length of chord
$N_{1,Rd}$	Design value of the joint capacity expressed as a brace load
T	Wall thickness of chord
P_{20}	Joint strength at ambient temperature
P_θ	Joint strength at elevated temperature
Q_f	Function to take account of the effect of chord stress in the connecting face
Q_u	Function in the design strength equations accounting for the effect of geometric parameters
b	Smaller diameter of brace member
d	Larger dimension of brace member
f_k	Buckling stress for chord side wall failure
f_{y0}	Yield stress of chord member
$k_{E,\theta}$	Reduction factors for modulus of elasticity at temperature θ
$k_{y,\theta}$	Reduction factor for yield strength at temperature θ
l	Length of brace
n	Chord pre-stress parameter
t	Wall thickness of brace
β	Diameter ratio (=d/D)
θ	Brace-to-chord intersection angle
θ_i	Included angle between brace member i and the chord
γ	Half width to thickness ratio of the chord (=D/2T)
η	Brace depth d (in direction chord axis) to chord width B ratio
ε_T	The true strain
ε	The engineering strain
σ_T	The true stress
σ	The engineering stress

a) NEO Bankside, London, UK [9] b) Odeon Cinemas, Liverpool, UK [15]

Fig. 1. Examples of EHS applications.

were subjected to either compressive or tensile forces. They carried out both experimental and numerical investigations on the behaviour of welded EHS T- and X-joints at ambient temperature. They concluded that the behaviour of EHS X-joint types 1 and 2 (see Fig. 1) were similar to that of RHS joints, whilst EHS X-joints types 3 and 4 could be treated as equivalent CHS joints, and proposed a new method to calculate the joint strength. However, Haque and Packer [14] performed twelve tests to investigate the effects of joint orientation, brace-chord angle and brace loading on the static strength of EHS X- and T-joints. It was found that the equivalent RHS approach was able to predict the capacity of these joints better than the equivalent CHS approach. This may be because an EHS joint has different behaviours in two different directions as an RHS joint and the wider side of an EHS is close to being flat. Moreover, in those studies mentioned above, it was noted that the load – displacement curves did not present a definite peak in some cases. Hence, the joint resistance was defined as the maximum axial force in the brace with a defined joint deformation limit. This will be explained in detail in the next section.

Till date, limited research exists investigating the effects of chord pre-stress (n) on tubular joint strength at elevated temperatures as per the authors' literature review. Shao et al. [16] tested six specimens to examine the influence of chord compressive pre-stress on maximum load carrying capacity of CHS T-joints at elevated temperatures. Feng and Young [17] conducted numerical simulations on T- and X-joints with compressive pre-stress in chord members. They reached similar research findings as Nguyen et al. [18] that chord compressive pre-stress significantly affects

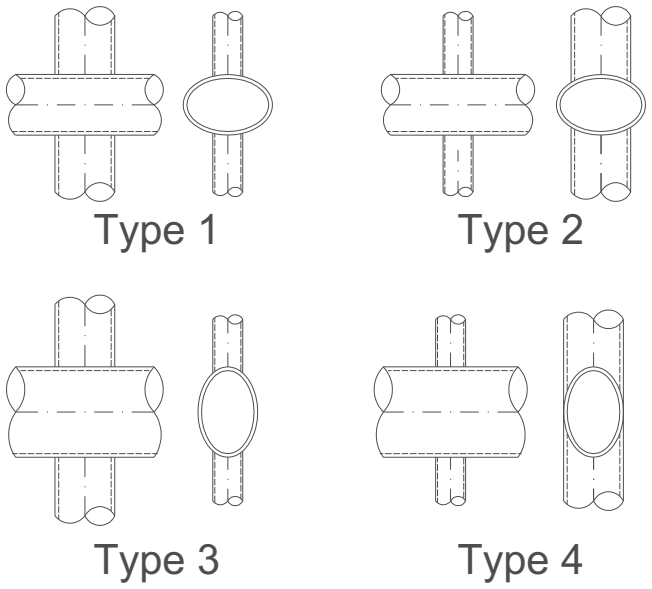

Fig. 2. EHS Joint orientations [7].

the maximum load carrying capacity of CHS T-joints at temperature higher than 400 °C and the current Eurocode EN 1993-1-8 [19] and CIDECT guide No. 1 [20] design guides overestimated capacities of the tested specimens at higher temperature. It seems that chord pre-stress can have significant effect on EHS joint resistance at higher temperature and this effect will be evaluated in this research.

Table 1 Summarises the main investigations at ambient temperature, indicating that EHS T- and X-joints of orientations 1, 2, 3 and 4 with the brace member in tension or compression have been investigated.

The investigations in Table 1 form the basis of the current design approach for EHS joints. In Eurocode EN 1993-1-8 [19] or CIDECT guide No. 3 [23], the current design method for calculating the ultimate strength of EHS joints at ambient temperatures is based on the equivalent rectangular hollow section (RHS) method. In this method, it is assumed that the EHS is an equivalent RHS, with a RHS width and depth equal the EHS smaller and larger diameters respectively. However, Packer et al. [24], Zhao et al. [25] and Haque et al. [22] defined the equivalent RHS as an RHS with width equal to the EHS small diameter and a depth that gives the same cross sectional area of the EHS.

Table 3
Chord side wall failure for all EHS joint types.

Eurocode EN 1993-1-8 [19]	CIDECT guide No. 3 [23]	Packer et al. [13]
$N_{1,Rd} = f_k TQ_f\left(\frac{2d}{\sin\theta_1} + 10T\right)$		$N_{1,Rd} = f_k Tb_w \frac{Q_f}{\sin\theta_1}$ $b_w = 2C(0.4d + 5T)$ With C = 1.1 for X-joints and 1.0 for T-joints
Compression: $Q_f = 1.3 - \frac{0.4n}{\beta}$ Tension: $Q_f = 1$	$Q_f = (1 - \lvert n\rvert)^{C_1}$ Compression: $C_1 = 0.10$ Tension: $C_1 = 0.10$	$Q_f = (1 - \lvert n\rvert)^{C_1}$ Compression: $C_1 = 0.10$ Tension: $C_1 = 0.10$

Table 4
Chord plastification for EHS Type 3 and 4 T- and X-joints, according to Packer et al. [13].

T joints	X joints
$N_{1,Rd} = C\left(\frac{1 + 6.8\beta^2}{1 + \beta}\right)\gamma^{0.20}\frac{f_{y0}T^2}{\sin\theta_i}Q_f$ With C = 6.4 for Type 3 and 4.8 for Type 4 $Q_f = (1 - \lvert n\rvert)^{C_1}$	$N_{1,Rd} = \frac{C}{1 - 0.7\beta}\gamma^{0.15}\frac{f_{y0}T^2}{\sin\theta_i}Q_f$ With C = 6.6 for Type 3 and 5.5 for Type 4
Compression: $C_1 = 0.20$ Tension: $C_1 = 0.15$	

Table 1
Summary of research on EHS joints at ambient temperature.

Joint type	Brace loading	Orientation type (see Fig. 2)	θ	Failure mode	References
X and N	Tension or compression	1	90°	Chord plastification in compression, chord yielding in tension	Bortolotti et al. [5] and Pietrapertosa et al. [6]
X and T	Tension or compression	1, 2, 3 and 4	90°and 45°	Chord tear-out or plastification for tension, chord plastification for compression	Shen et al. [8,10,11,21], Packer et al. [13] and Wardenier et al. [12]
X and T	Tension or compression	1, 2 and 3	90° and 45°	Chord plastification for type 1, chord sidewall failure for type 2 and 3. Chord tear out, sidewall or brace failure for tension	Haque et al. [22]

Table 2
Chord plastification for Type 1 and 2, T- and X-joints.

Eurocode EN 1993-1-8 [19]	CIDECT guide No. 3 [23]	Packer et al. [13]
	$N_{1,Rd} = Q_u Q_f \frac{f_{y0}T^2}{\sin\theta_i}$	
$Q_u = \frac{2\eta}{(1-\beta)\sin\theta_1} + \frac{4}{\sqrt{1-\beta}}$		$Q_u = C*\left(\frac{2\eta}{(1-\beta)\sin\theta_1} + \frac{4}{\sqrt{1-\beta}}\right)$ With C = 0.9 for X-joints and 1.1 for T-joints
Compression: $Q_f = 1.3 - \frac{0.4n}{\beta} \le 1$ Tension: $Q_f = 1$	$Q_f = (1 - \lvert n\rvert)^{C_1}$ Compression: $C_1 = 0.60–0.5\beta$ Tension: $C_1 = 0.10$	$Q_f = (1 - \lvert n\rvert)^{C_1}$ Compression: $C_1 = 0.20$ Tension: $C_1 = 0.15$

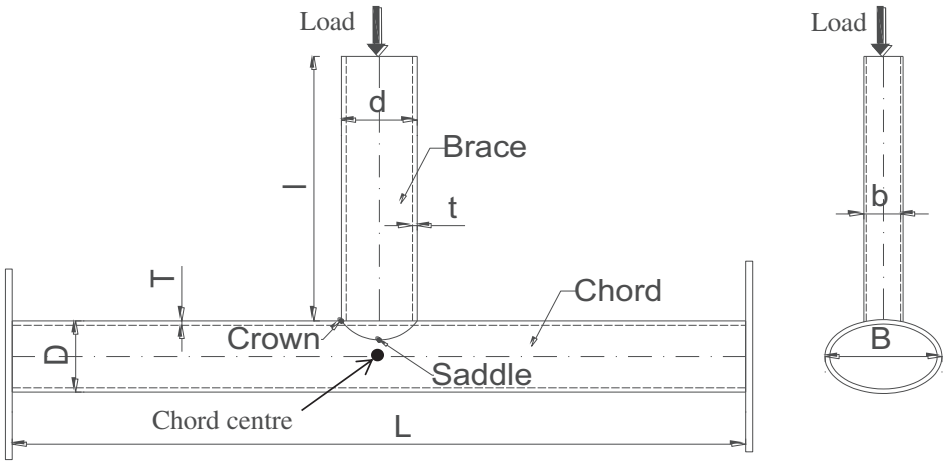

Fig. 3. Typical arrangement and geometrical parameter definitions for EHS T-joint [13].

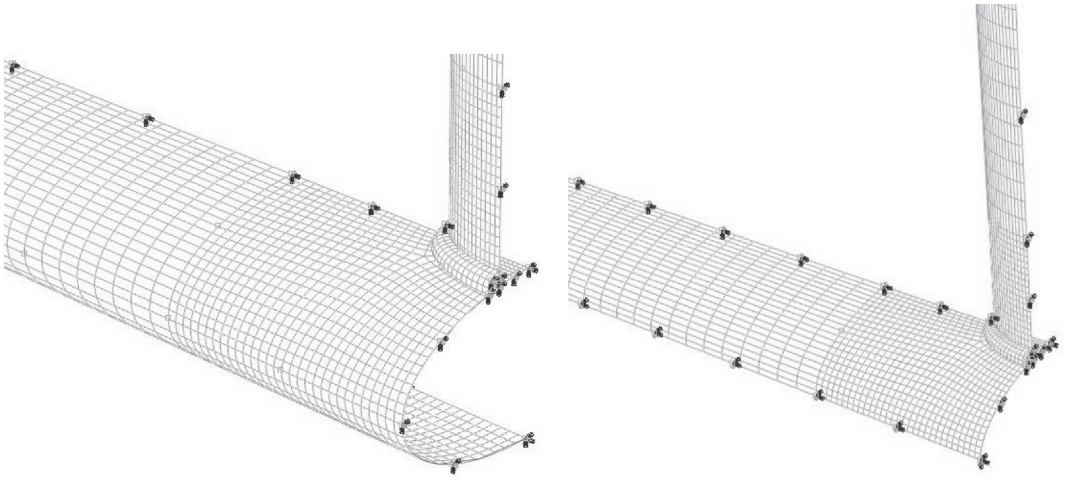

a) EHS T-joint b) EHS X-joint

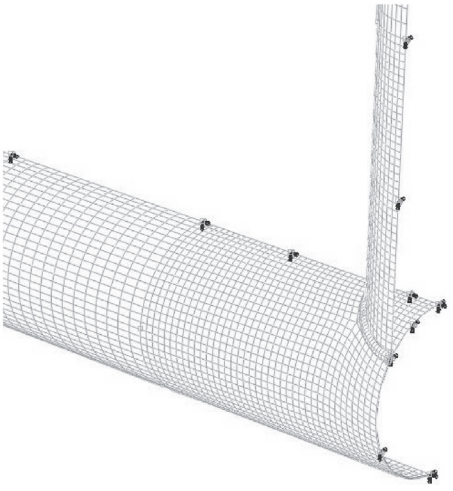

c) CHS T-joint

Fig. 4. Mesh layouts for T- and X-joints.

Table 5
Packer et al. [13] and Tan et al. [28] joint test specimens used for FE model validation.

Joint ID	D (mm)	d (mm)	B (mm)	b (mm)	T (mm)	t (mm)	L (mm)	l (mm)
T90-1C-UT	220	110	110	220	5.94	5.94	1098	1089
T90-2C-UT	220	220	110	110	5.94	5.94	1098	1042
T90-3C-UT	110	110	220	220	5.94	5.94	1100	1032
X90-1C-UT, X90-1T-UT, X45-1C-UT	220	110	110	220	5.94	5.94	2193	1089
X90-2C-UT, X90-2T-UT, X45-2C-UT	220	220	110	110	5.94	5.94	997	1043
X90-3C-UT, X90-3T-UT, X45-3C-UT	110	110	220	220	5.94	5.94	1016	989
PT1	244.5	193.7	–	–	6.3	6.3	2200	1100
PT3	244.5	168.3	–	–	6.3	6.3	2200	1100
PT5	244.5	114.3	–	–	6.3	6.3	2200	1100

The RHS joint strength equations of RHS are then used to determine the capacity of EHS joints. Shen et al. [8–11], Wardenier et al. [12] and Packer et al. [13] have proposed alternative EHS joint strength calculation equations.

Tables 2–4 compare the proposed equations of Packer et al. [13] with the CIDECT guide No. 3 [23] and Eurocode EN 1993-1-8 [19] design guide equations for EHS T- and X-joints of different types (1, 2, 3 and 4) and joint failure modes. Q_u is a design strength function without chord axial stress, and Q_f is a chord stress function (reduction factor parameter) for reducing the connection resistance due to chord stress. A relationship exists between the proposed equations of Packer et al. [13] and the current design guide equations. Indeed, a modification factor in the CIDECT guide No. 3 [23] and Eurocode EN 1993-1-8 [19] design guide equations, which are used for calculating the ultimate strength of RHS joints, is necessary to predict the capacity of EHS joints.

These previous research studies indicate that even at ambient temperature, there are inconsistencies in calculating EHS joint static strength using an equivalent RHS joint approach. This study will add further numerical modelling results for additional assessment of the ambient temperature design approach.

An extensive search by the authors has revealed that there is no direct research on EHS joints at elevated temperatures. Relevant research studies on welded tubular joints at elevated temperatures are presented in [4,16,26–29]. In Ozyurt et al. [4], based on extensive numerical simulations of different types of Circular (CHS) and Square Hollow Section (SHS) joints, the authors proposed a design method for calculating the static resistance of SHS and CHS joints at elevated temperatures, by applying material modification factors to the ambient temperature equations. For T-, Y- and X-joints with the brace member in tension, in which joint failure is controlled by steel strength, the elevated temperature steel yield strength reduction factor should be applied to modify the ambient temperature calculation method. For T-, Y- and X-joints with the brace member in compression, where excessive ovalisation of the chord at elevated temperatures changes the joint geometry, the ambient temperature joint strength equations should be modified by the elevated temperature reduction factor for Young's modulus of steel. This study will investigate whether the above outlined method of the authors can be extended to predict the capacity of welded EHS T- and X-joints, considering different orientation types, joint configurations and brace loading at higher temperatures.

Due to a lack of experimental data, the results of this numerical study are based on simulations using the commercial finite element software ABAQUS [30]. The adopted simulation model in this study has already been checked to be able to simulate the behavior of SHS and CHS joints at both ambient and elevated temperatures in Ozyurt et al. [20,26] previously. In this finite element study, validation results to demonstrate efficacy of the simulation model adopted for replicating the behavior of EHS joints but only at ambient temperature conditions are reported due to lack of experimental data available for EHS joints at elevated temperature conditions.

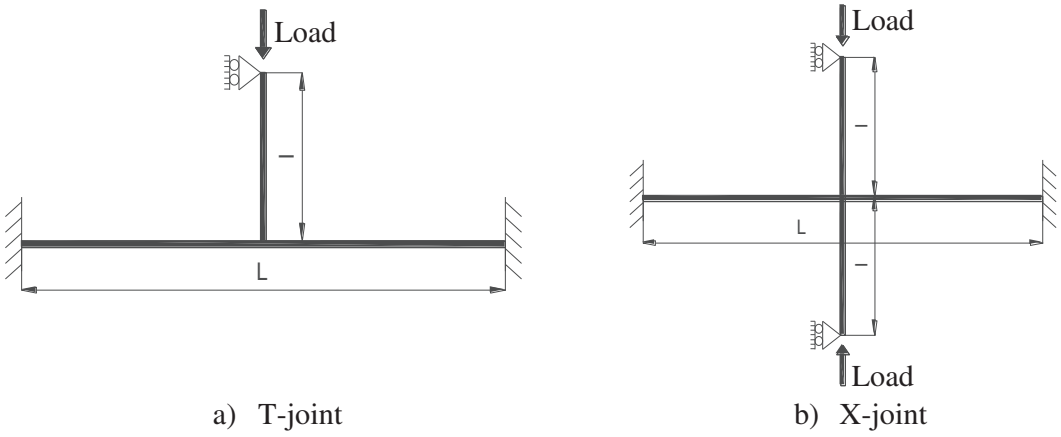

Fig. 5. Loading and boundary conditions of Tan et al. [28] and Packer et al. [13] joint tests.

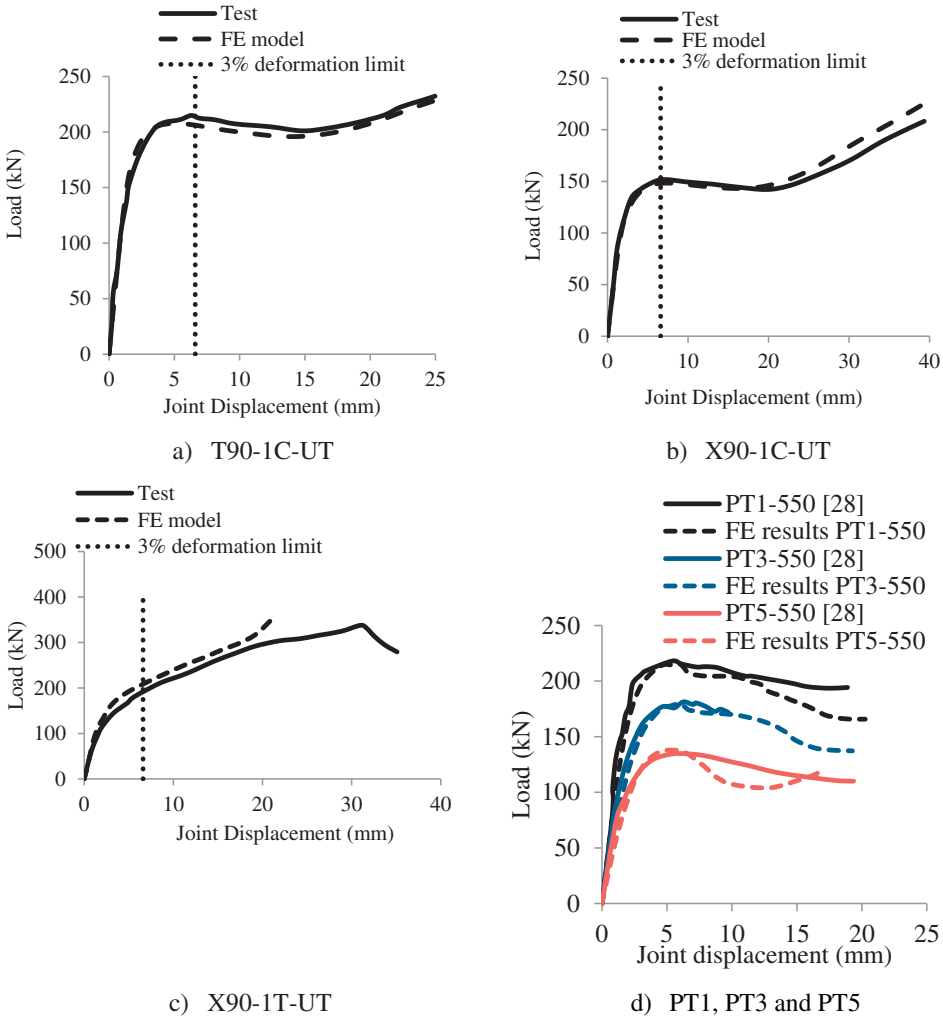

Fig. 6. Comparison for load–displacement curves.

2. Description of the finite element model and further validation results

The experimental results of Packer et al. [13] on EHS T- and X-joints at ambient temperature and the test results of Tan et al. [28] on CHS T-joints at elevated temperatures, which is a special case of EHS, are used for validation of the numerical model. Fig. 3 shows the geometric configuration of a typical EHS T-joint. To reduce computational time, only a quarter of T-joint, either a quarter or eighth of X-joint (depending on the brace angle) will be modelled to take advantage of symmetry in geometry and loading by applying appropriate boundary conditions for symmetry. Fig. 4 shows typical numerical models for T- and X-joint.

The same modelling parameters, as used by Ozyurt et al. [4,31] in their investigations of CHS and SHS joints, were adopted to model EHS joints. In the ABAQUS simulation models, quadrilateral thick shell (S8R) elements were used for both the chord and brace members for accuracy and computational efficiency; quadratic wedge solid elements (C3D20) were used for welds for accurate meshing. The ABAQUS sweep function was used to model the weld geometry.

For the EHS T- and X-joints tested by Packer et al. [13], the steel grade was S355 with a nominal yield strength = 402 N/mm^2 and an ultimate strength = 517 N/mm^2 from their coupon test results. The elastic modulus of steel was assumed to be 210 GPa.

For the CHS T-joints tests performed by Tan et al. [28], the nominal yield strength, the ultimate yield strength and the elastic modulus of steel were 380.3 N/mm^2, 519.1 N/mm^2 and 201.2 GPa respectively. This study also used the material properties at elevated temperatures were also used from the test results of Tan et al. [28].

In the ABAQUS simulation model, the true stress–strain curve was input after converting the engineering stress–strain curve into the true stress and logarithmic strain curve [32].

$$\varepsilon_T = \ln(1 + \varepsilon) \quad (1)$$

$$\sigma_T = \sigma.(1 + \varepsilon) \quad (2)$$

where

ε_T, is the true strain
ε, is the engineering strain
σ_T, is the true stress
σ, is the engineering stress

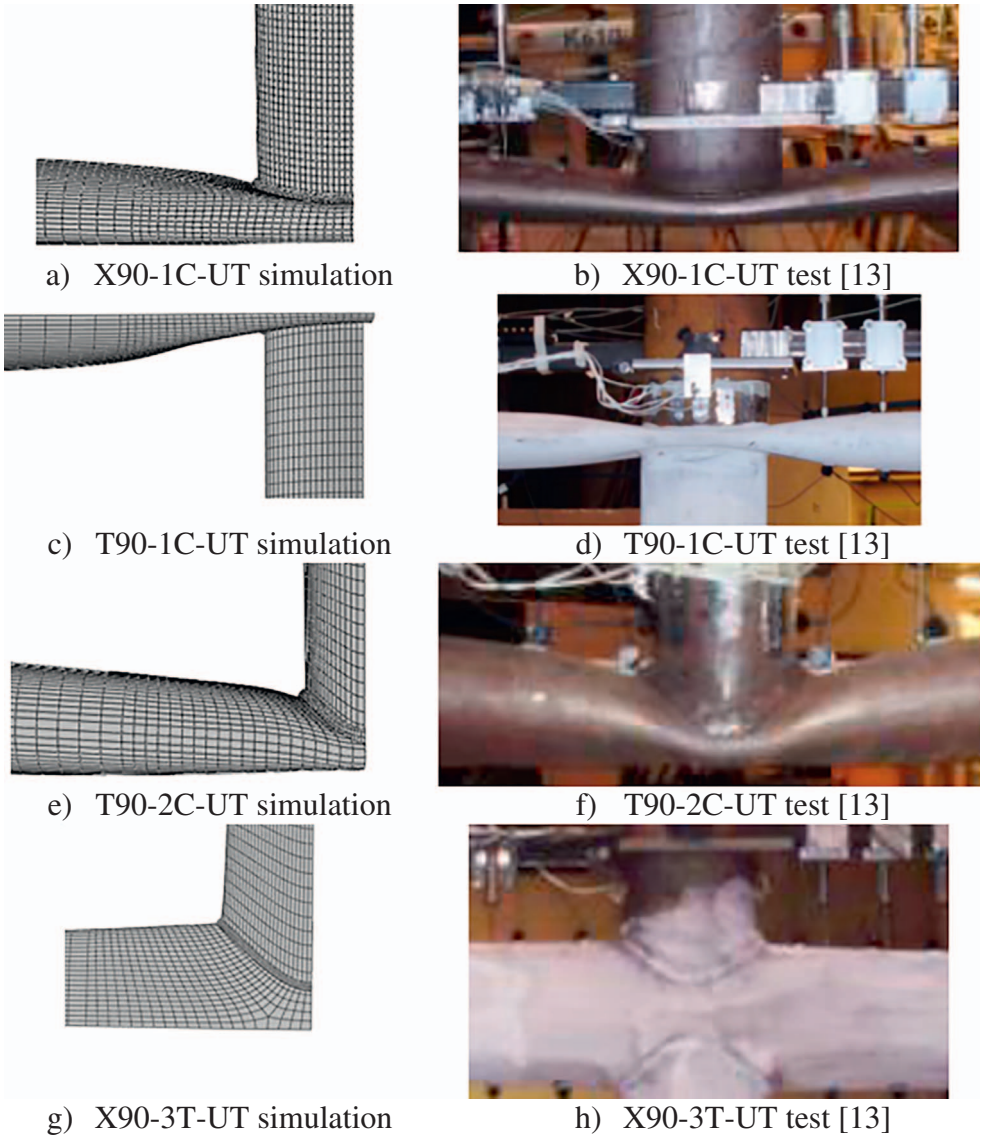

Fig. 7. Deformed shapes of selected X- and T-joints at ambient temperature.

In all numerical analyses, the Von-Misses yield surface criterion and isotropic strain hardening rules were used.

A mesh convergence study, based on test T90-1C-UT of Packer et al. [13] was carried out to determine a suitable FE mesh size which was then applied to all models. Mesh sizes of 10 mm and 5 mm were found to be suitable for the tubular members and the weld. Outside the joint zone, a coarse mesh (20 mm) can be used.

The brace and chord members were tied with the weld elements using the ABAQUS "tie" function. Discretization method was defined as surface to surface contact. The brace and chord members at the connection region were chosen as a master surface, while the weld elements were slave surface.

There are two methods to apply the mechanical loads in ABAQUS: Static and Riks methods. In order to examine the effects of large deformations in joints after reaching the maximum load, the Riks method was chosen.

Three different orientations of EHS T- and X-joints of Packer et al. [13]and three specimens of CHS T-joints of Tan et al. [28] were simulated. The EHS T-joints are Tests T90-1C-UT, T90-2C-UT and T90-3C-UT under compressive brace member. For EHS X-joints, type 1, 2 and 3 configurations had two different angles between the brace and chord members (45° and 90°). For the CHS T-joints, PT1, PT3 and PT5 were modelled with compressive brace member. Unfortunately, there were no test results for EHS joints with chord pre-stress (pre-load). However, Ozyurt et al. [26] has presented validation study on CHS joints under elevated temperature conditions with chord pre-stress previously. Table 5 summarises the simulated joints and their dimensions and Fig. 5(a) and (b) show their loading and boundary conditions. Since imperfections have negligible effects on joint strength [13], the joints were modelled with the dimensions in Table 5 without imperfections. Only the behaviour of the joints prior to crack initiation and fracture is simulated in the current finite element study.

The behaviour of tubular joints primarily depends on the local deformation of the connection area when premature failure at brace

Table 6
Comparison between numerical results and the test data of both Packer et al. [13] and Tan et al. [28] for the strength of T- and X-joints.

Joint name	Simulation results (kN)	Test results (kN)	Simulation/test
T90-1C-UT	205.6	216.5	0.95
T90-2C-UT	359.7	353.0	1.02
T90-3C-UT	602.1	593.8	1.05
X90-1C-UT	145.3	150.5	0.95
X90-2C-UT	547.8	539.7	1.03
X90-3C-UT	561.2	555.1	1.03
X90-1T-UT	194.0	187.9	1.05
X90-2T-UT	581.3	567.0	1.03
X90-3T-UT	1205.5	1188.8	1.04
X45-1C-UT	269.0	258.5	1.04
X45-2C-UT	645.5	627.8	1.03
X45-3C-UT	743.3	701.0	1.06
PT1	215.5	216.5	1.00
PT3	179.6	180.9	0.99
PT5	137.8	133.7	1.03
Mean	N/A	N/A	1.02
Standard deviation	N/A	N/A	3%

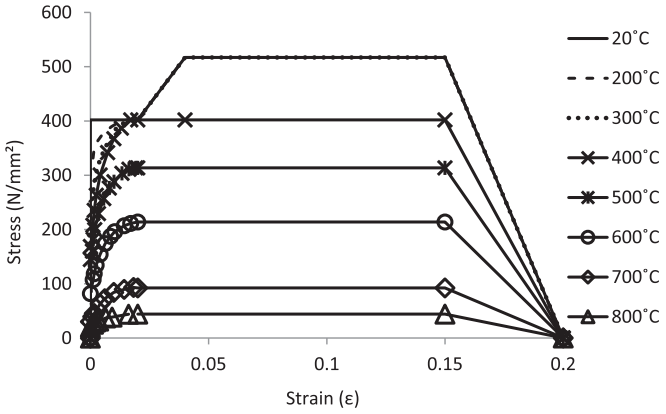

Fig. 8. Engineering stress-strain relationships of S355 grade steel at elevated temperatures (according to EN 1993-1-2 [36]).

Table 7
Geometrical parameters for T- and X-joints, Types 1, 2, 3 and 4.

Joint dimension identifier	D	B	T	d	b	t	L	l	β	θ
	(mm)								(d/D)	(°)
1	250	125	8	150	75	5	1500	600	0.60	90
2	250	125	8	120	60	5	1500	600	0.48	90
3	300	150	10	250	125	10	2000	1000	0.83	90
4	300	150	8	150	75	6.3	1800	600	0.50	90
5	300	150	8	120	60	5	1800	600	0.40	90
6	400	200	10	200	100	10	2500	1000	0.50	90
7	400	200	10	150	75	6.3	2500	1000	0.38	90
8	400	200	8	120	60	8	2500	1000	0.30	90
9	250	125	8	120	60	5	1500	600	0.48	30
10	250	125	8	120	60	5	1500	600	0.48	45
11	250	125	8	120	60	5	1500	600	0.48	60

member and weld is prevented. Therefore, a deformation limit should be based on the local deformations of the chord at the intersection between brace and chord members. The resistance of EHS joints (also referred to as joint strength) corresponds to the load at the maximum deformation limit of 3%D (0.03D), as defined by Lu et al. [33] and

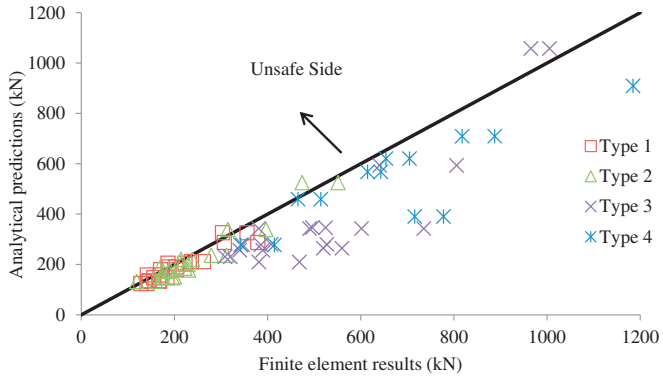

a) Eurocode 3 EN-1993-1-8 [19] equivalent RHS method

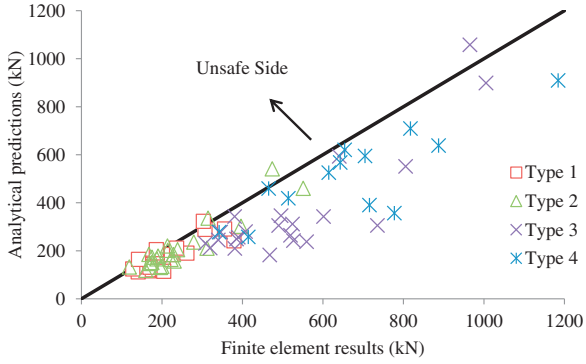

b) CIDECT guide No. 3 [23] equivalent RHS method

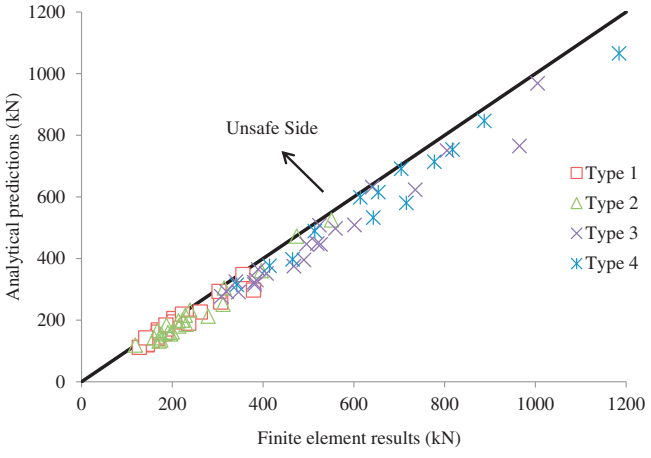

c) Packer et al. [13] EHS method

Fig. 9. Comparison for joint strength between numerical simulation results and different design methods at ambient temperature

adopted by various researchers [8,9,12,13,16,26] for tubular joint strength calculation, or the maximum load, whichever occurs first.

Fig. 6 shows a comparison between selected experimental load-displacement curves of Packer et al. [13] and Tan et al. [28] with numerical simulation results of the finite element analyses carried out in the validation study herein. The maximum deformation limit is

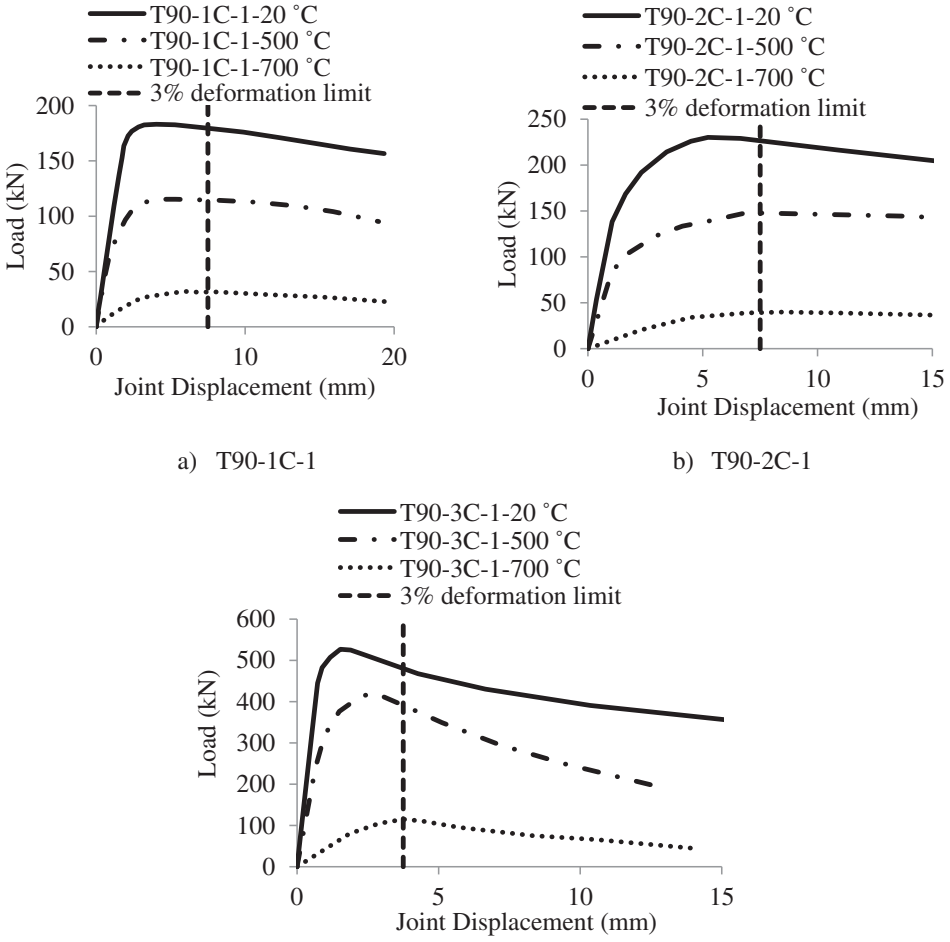

Fig. 10. Comparison for load-displacement curves at different temperatures.

indicated in Fig. 6(a–c). Joint displacement in Fig. 6 refers to local indentation of the chord face, which is the vertical axial displacement of the brace with respect to the chord centre and load refers to that applied in the brace as shown in Fig. 3. Fig. 7 compares typical deformed shapes between numerical simulation and test of Packer et al. [13] for representative cases, showing close matching of the results. Table 6 compares the ultimate capacity of the joints between simulation and test results. The numerical simulation results are in good agreement with the test results, with an average simulation result/test result ratio of 1.02 and a standard deviation of 3%. Since there are no available test results for EHS joints at elevated temperatures, it is not possible to directly validate the numerical simulation model. However, the validation results presented here for EHS joints at ambient temperature conditions combined with validity of the CHS joints at elevated temperatures, which is a special case for EHS joints, suggest that the adopted finite element model is considered suitable for simulating the behavior of EHS joints further in this study at elevated temperature conditions.

3. Parametric study and results

The validated FE model was used to investigate the behaviour and strength of axially loaded EHS T- and X-joints for the four different orientations shown in Fig. 2 at different temperature levels. A total of four hundred sixteen simulations were performed to evaluate the effects of elevated temperatures. First, the numerical simulation results at ambient temperatures are used to assess the current design equations of CIDECT guide No. 3 [23] and Eurocode 3 EN-1993-1-8 [19] and the alternative design equations of Packer et al. [13] to identify a more suitable one as the basis for calculating elevated temperature joint resistance. Afterwards, elevated temperature simulation results are used to assess how to modify the ambient temperature calculation method for elevated temperature applications, following the suggestion of Ozyurt et al. [4]. Fig. 5 shows boundary conditions of FE models. Previous studies [8–13] have shown that the chord end restraint conditions have limited effect on joint strength as long as the length of the chord member is at least six times longer than the external width of the EHS section. Although there is no research on whether this assumption remains acceptable for EHS joints at elevated temperatures, previous studies [27,34,35]suggests that chord end effects are minimal provided the chord length is at least 6D at elevated temperatures too. Where, D is the wider dimension of EHS chord.

For elevated temperature simulations, steady state condition was assumed for convenience, in which temperatures of the structure were

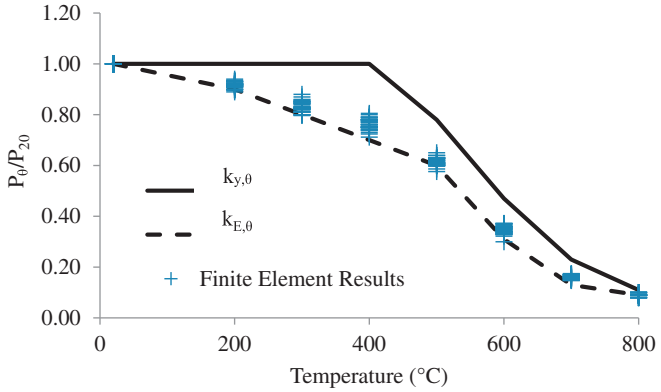

a) EHS T- and X-joints Type 1 and 2

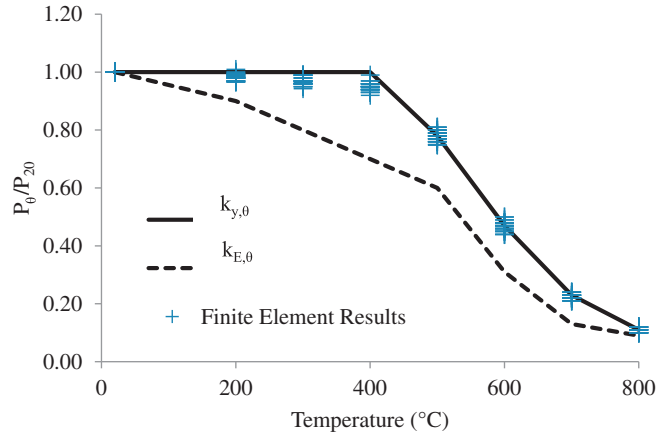

b) EHS T- and X-joints Type 3 and 4

Fig. 11. Comparison for EHS T- and X-joint strength reduction at elevated temperatures for different joint orientations.

raised to the required level and mechanical loading was then applied. Ozyurt et al. [4] previously confirmed that the static and transient simulation results were very close. Both geometry and material non-linearities were included. In order to examine large deformation behaviour, the RIKS method was chosen. When the arc length increments were within the maximum and minimum limitations of 0.1 and 1E-08 respectively, numerical convergence was considered to have been achieved.

For the weld material, the same material properties of chord and brace members were used (Fig. 8). Uniform temperature distribution was assumed for both the chord and brace members. However, Lan et al. [29] suggested that the weld is having insignificant effect on joint strength. As this study is focused on chord face plastification, the heat affected zone is not considered critical.

For identification of the simulated cases, the designation is L1N1-N2L2-N3: The first letter (L1 = T or X) indicates joint type. The first number (N1 = 30, 45, 60 or 90) represents the angle between the brace and chord members. The second number (N2 = 1, 2, 3 or 4) indicates the joint orientation as shown in Fig. 2. The next letter (L2 = T or C) represents the brace loading direction (Tension or Compression). The last number (N3) identifies the geometrical parameters from Table 7. For example, T90-1C-1 means T-joint type 1 with the brace - chord angle 90 degree under brace axial compression load for joint 1 dimensions according to Table 7. The joint dimensions in Table 7 cover practical ranges of brace to chord diameter ratio (β), half width to thickness ratio of the chord (γ = D/2T) and connection angle.

3.1. Assessment of calculation methods for strength of EHS joints at ambient temperature

Fig. 9 summarises the comparison between simulation results with predictions of three different analytical methods: the CIDECT guide No. 3 [23] equivalent RHS method, the Eurocode 3 EN-1993-1-8 [19] equivalent RHS method and the method of Packer et al. [13], details of which are presented in Tables 2–4. Detailed results are provided in Appendix Tables A.1–A.4. Fig. 9(a) and (b) indicate that both the CIDECT guide No. 3 [23] and Eurocode 3 EN-1993-1-8 [19] equivalent RHS member approaches can give grossly inaccurate results for Type 3 and 4 EHS joints, with the design equations generally overestimating joint strength, while these methods give better accuracy for Type 1 and 2 EHS joints. However, the proposed method of Packer et al. [13] gives the most satisfactory results in all cases. These results are in accordance with the proposals of [8–11,13] that the strength equations of EHS T- and X-joints can be adapted from those of CHS and RHS joints, but modification factors, as suggested by Packer et al. [13] should be adopted.

3.2. Effects of elevated temperatures, brace in compression

Eighty cases were generated at various temperatures (20, 200, 300, 400, 500, 600, 700 and 800 °C) to evaluate the effects of elevated temperatures. As at ambient temperature, the strength of EHS joints is based on the maximum displacement limit of 3%D (0.03D), as defined by Lu et al. [33]. Fig. 10 illustrates selective load-displacement curves at different temperatures for one EHS T-joint. As shown in Fig. 10, the peak load of EHS joint was either reached before the displacement limit or the joint load changed little after the 3% displacement limit.

Fig. 11 compares the ratios of elevated temperature joint strength, P_θ to ambient temperature joint strength, P_{20} with steel yield strength or Young's modulus reduction factors at elevated temperatures. From Fig. 11(b), it can be seen that for Type 3 and 4 joint orientations, using the elevated temperature reduction factors for steel yield strength to modify the ambient temperature equation of Packer et al. [13] gives accurate calculations of elevated temperature joint strength. For Type 1 and 2 joints, using the reduction factors for steel yield strength would give higher, and hence the results are unsafe as illustrated in Fig. 11(a). Using the elevated temperature reduction factors for steel Young's modulus produces much better agreement with the simulation results.

This can be explained by the effects of changing geometry of EHS joints of different orientations at higher temperatures, similar to the phenomena observed by Ozyurt et al. [4] for CHS and SHS joints at elevated temperatures. For EHS orientations 1 and 2 where the larger diameter (flatter) side of the EHS is loaded under a compressive force in the brace, the chord wall experiences large local deformations as shown in Fig. 12, thus (i) imposing an extra bending moment due to the local P- δ effect and (ii) flattening of the chord surface causing the yield line capacity of the chord face to decrease compared to the undeformed chord face. Since this phenomenon is a result of large deformation, using the reduction factor for steel Young's modulus is appropriate, as confirmed by the results in Fig. 11(a).

In contrast, for EHS joint configurations 3 and 4, because the narrower side of the chord is loaded, the chord is rigid and hence experiences very small local deformations and flattening, as shown in Fig. 13.

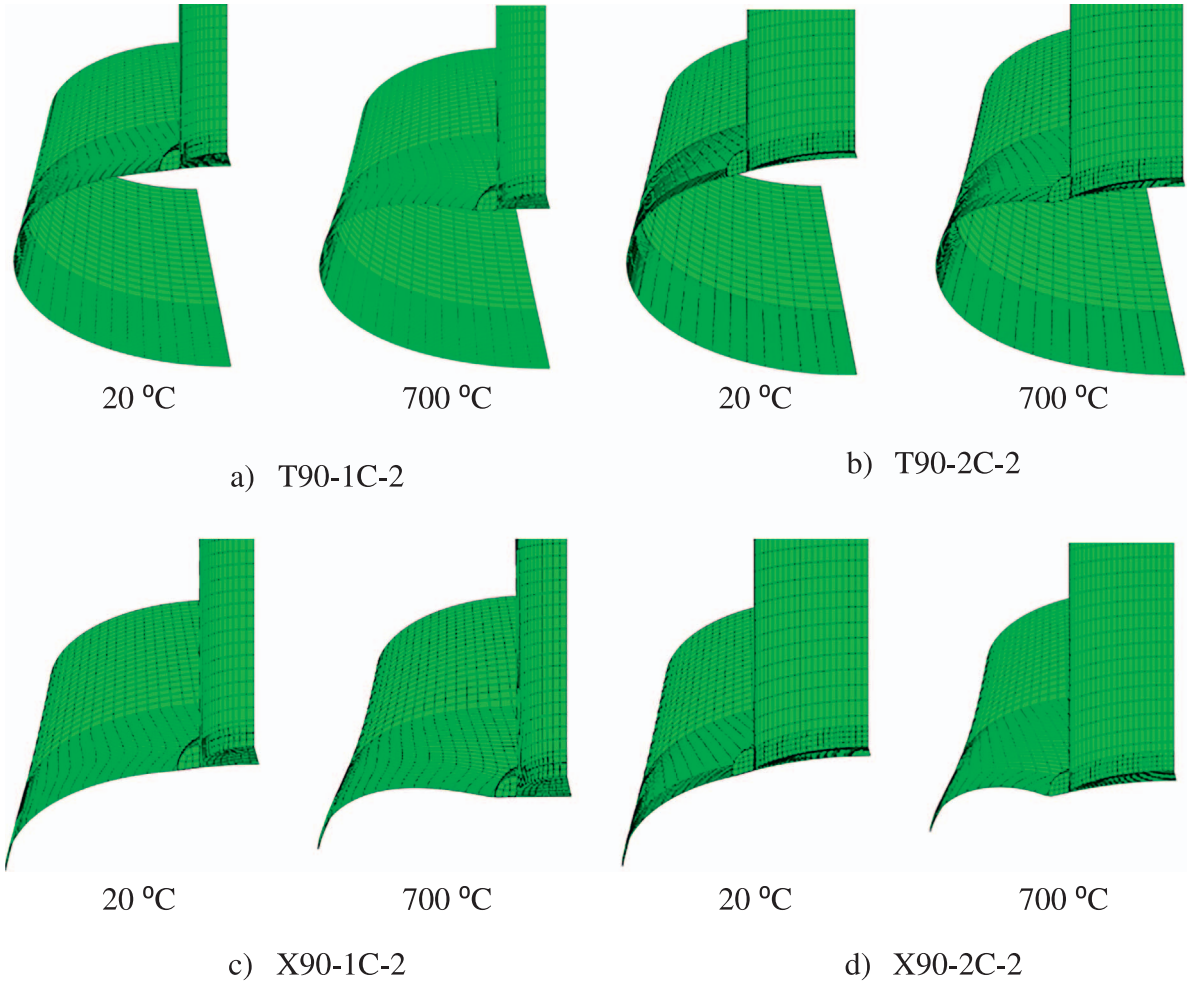

Fig. 12. Deformed shape of T- and X-joints (Orientations 1 and 2) at ambient and elevated temperatures.

Therefore, the joint failure mode at elevated temperatures is the same as at ambient temperature. Hence, the steel yield strength reduction factor should be used as the modification factor for calculating joint strength, as supported by the results in Fig. 11(b).

In consideration of various geometrical parameters, which are summarised in Table 7, the effects of connection angle and half width to thickness ratio of the chord (γ) on joint strength ratio are investigated. Fig. 11 reveals that there is a similar trend in the joint strength ratios for different connection angles and γ at elevated temperatures. These results are consistent with the findings of Tan et al. [28] which show that the influence of chord thickness on joint strength ratios is independent of temperature.

3.3. Brace in tension

For all EHS joints with the brace members in tension, the deformation behavior and failure mode at elevated temperatures are the same as at ambient temperature. When the brace is in tension, the local P-δ and chord face flattening effects disappear. Therefore, when calculating the elevated temperature joint strength, it is acceptable to use the elevated temperature steel yield strength reduction factor to modify the ambient temperature calculation equation. This is confirmed by the results in Fig. 14.

3.4. Effects of pre-stress in chord member

In this section, the effects of chord pre-stress on EHS joint strength at different temperatures, ranging from 20 °C to 700 °C are investigated. The chord pre-stress ratio (n, tension position) is defined as chord stress at the connection divided by the chord yield stress. The chord pre-stress ratio (n) was ± 0.2, ± 0.4, ± 0.6 and ± 0.8. The chord member was subjected to either a compression or tension force prior to loading the brace member. Therefore, two loading steps were generated in ABAQUS for X-joints. In the first step, loads were applied to the ends of the chord member. In the second step, the chord loads were kept constant and a load was applied to end of the brace member. For T-joints, the axial load in the brace induces in-plane bending moments in the chord member. In order to investigate actual chord stress ratio (n), EHS T-joints were applied compensating bending moments at the chord ends as shown Fig. 15(a) [13]. For this purpose, the magnitude of the chord end moments was dependent on the load applied at the loading ends of the brace member. The details of the numerical model for EHS T-joints with compensating bending moments are presented in Appendix B.

The joint dimension identifier 2 in Table 7 with four different orientations (from Type 1 to 4) was used for T- and X-joints in the parametric study. Fig. 15 illustrates the loading conditions when the chord member is in compression.

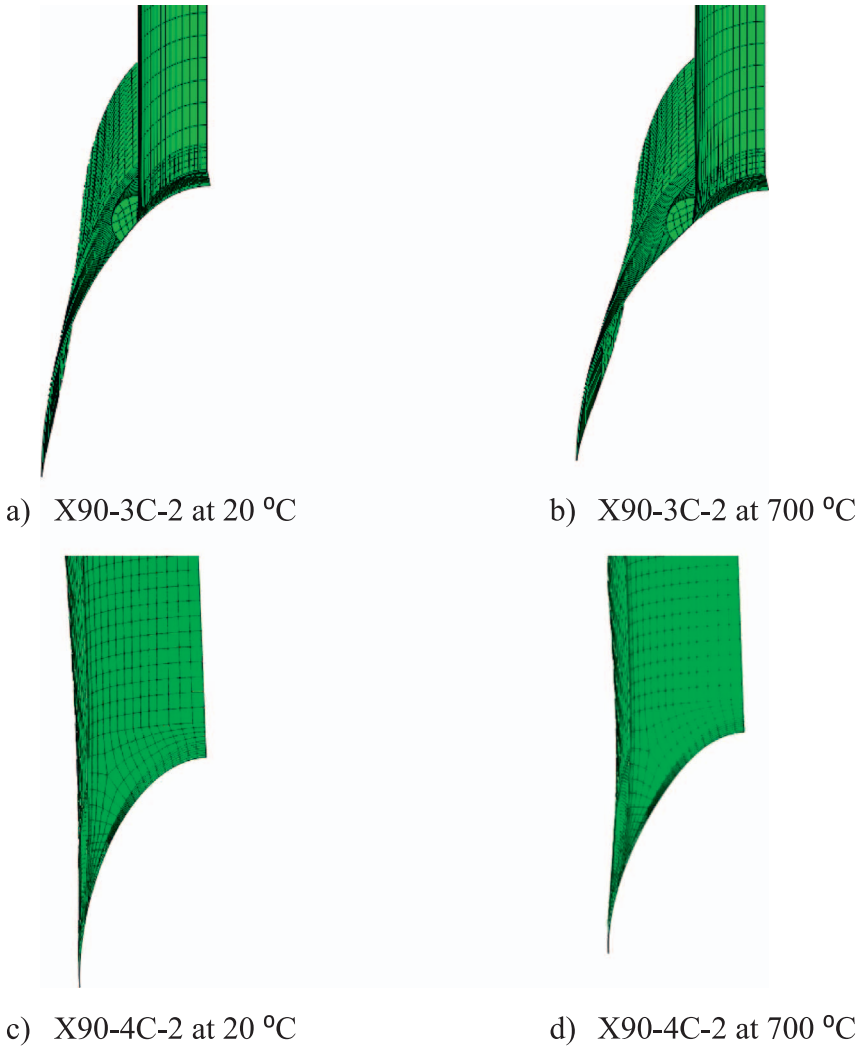

Fig. 13. Deformed shape of X-joints (Orientations 3 and 4) at ambient and elevated temperatures.

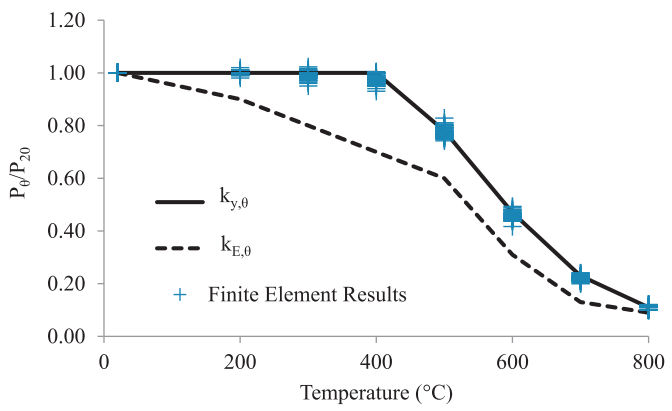

Fig. 14. Variations of EHS joint strength under brace in tension at different temperatures

Fig. 16 presents variations of chord pre-stress parameter (n) with the reduction factor (Q_f), defined as the ratio of joint strength with chord pre-stress in the connecting face to that without chord pre-stress in the intersection area for 20 °C and 700 °C, among the plots of numerical simulation outcomes, calculations using the CIDECT guide No. 3 [23], Eurocode 3 EN-1993-1-8 [19] design guides and the alternative approach of Packer et al. [13]. Appendix C provides further tabulated details. Detailed results of T- and X-joints with n = 0.0 and −0.4 for each orientation at 20 °C and 700 °C are provided in Appendix Tables C.1–C.2. With compressive pre-stress in the chord member, the results in Fig. 16(a), (b) and (c) show that the predictions of Packer et al. [13] are accurate, while using either CIDECT guide No. 3 [23] or Eurocode 3 EN-1993-1-8 [19] generally gives much lower joint resistance results as shown in Fig. 16(a) and (b). For Type 4 EHS joints (see Fig. 16(c)), both CIDECT guide No. 3 [23] and Packer et al. [13] calculation results are close to simulation results, with the Packer et al. [13] calculation results erring slightly on the safe side. Eurocode 3 [19] results are much higher than simulation results. These suggest that the CIDECT guide No. 3 [23] and Eurocode 3 EN-1993-1-8 [19] methods are inconsistent for different orientation types. When the chord is under tensile pre-stress, the simulation results indicate a detrimental effect of chord pre-stress, which is in accordance with the CIDECT guide No. 3 [23] and Packer et al. [13]. In contrast, Eurocode 3 EN-1993-1-8 [19] suggests that there is no substantial reductions in joint strength as shown in Fig. 16(a), (b) and (c). Furthermore, temperature has a negligible effect on the reduction factors for EHS T- and X-joints.

Therefore, the authors recommend to use the reduction factors of Packer et al. [13] when the chord member is subjected to either compressive or tensile pre-stress, as this method consistently gives accurate and safe predictions compared to simulation results.

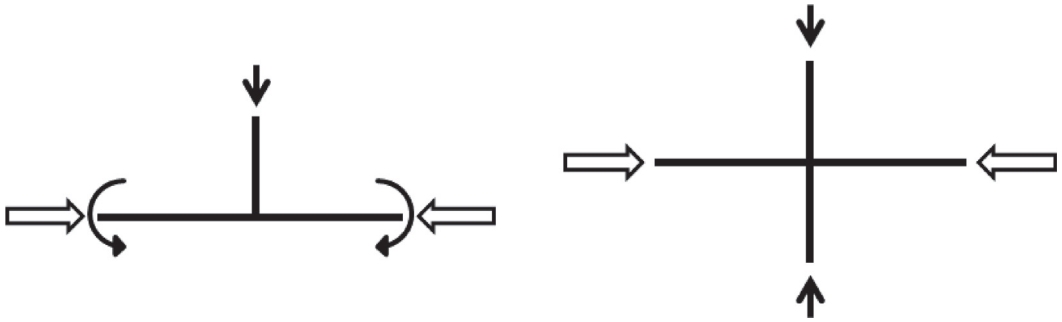

a) T90-1C-2 b) X90-1C-2

Fig. 15. Loading conditions of T- and X-joints with the chord member in compression.

4. Conclusions

This study has presented the results of an extensive parametric study on the strength of welded steel EHS joints at various temperatures. Finite element (FE) simulations of axially loaded elliptical tubular T- and X-joints at ambient temperature were first validated against available test results. The effects of different joint types, joint orientations, and chord pre-stress on EHS joint strength at both ambient and elevated temperatures were investigated to first identify a suitable ambient temperature design method and then to use the method as the basis for developing a design approach for elevated temperature applications.

Based on the numerical simulation results of this study, the following design recommendations are given:

(1) The modified equations suggested in Packer et al. [13] give more accurate results than those of CIDECT guide No. 3 [23] and EN 19931–8 [19].
(2) Furthermore, when the chord member is under a tensile pre-stress, it is not suitable to use the EN-1993-1-8 [19] equation - the joint strength decreases considerably as predicted by the proposed equations of CIDECT guide No. 3 [23] and Packer et al. [13]. When the chord pre-stress is compressive, the CIDECT guide No. 3 [23] and EN 1993–1-8 [19] design equations generally calculate much higher reduction factors except for type 4 joint orientation (connection to the EHS narrower face) compared to the simulation results. In contrast, the Packer et al. [13] method consistently gives accurate reduction factors for each joint orientation and is recommended to be used.
(3) For Type 1 or 2 joint orientations with brace in compression (connection to the EHS wider face) at elevated temperatures, the ambient temperature joint strength equation should be modified by the reduction factor of Young's modulus of steel.
(4) For Type 3 or 4 joint orientations with brace in compression (connection to the EHS narrower face) at elevated temperatures, the ambient temperature joint strength equation can be modified by the reduction factor of yield strength of steel.
(5) For all joint configurations with brace in tension at elevated temperatures, the ambient temperature joint calculation equation can be used, by changing the yield strength of steel at ambient temperature to that at elevated temperatures.

Acknowledgement

The authors would like to thank CIDECT for partial funding of the research of this paper through a CIDECT project 15U – Welded Joint Strength at Elevated Temperatures.

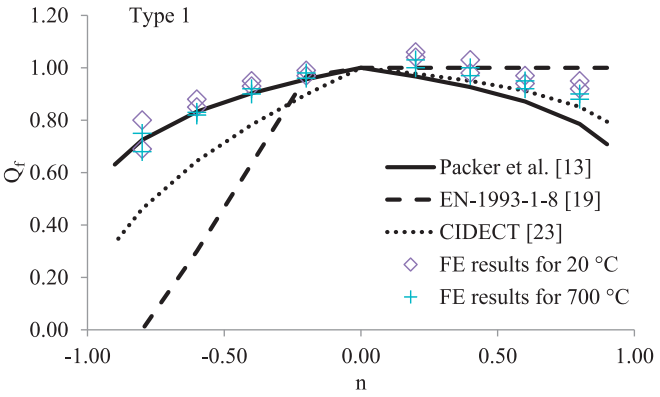

a) Type 1 (β=0.24)

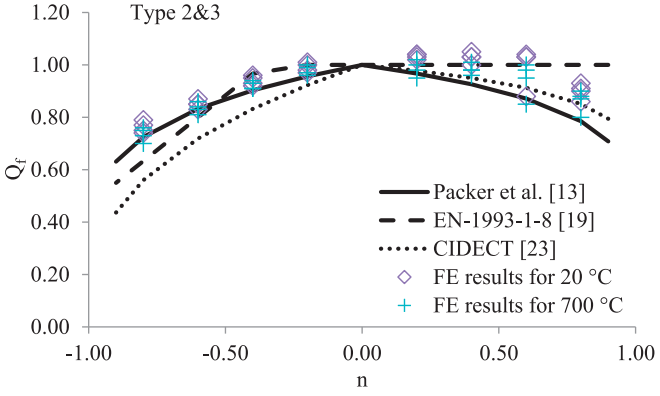

b) Type 2 and 3 (β=0.48)

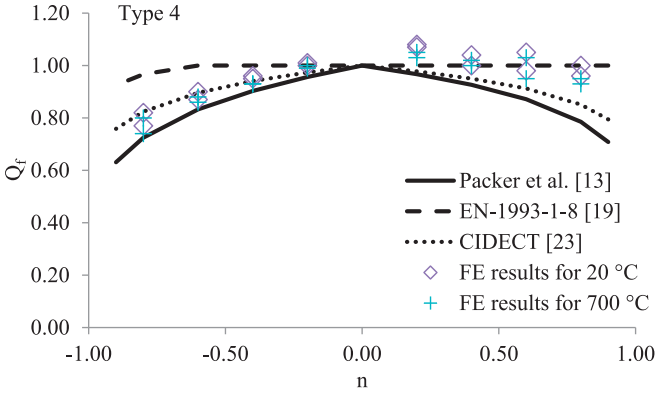

c) Type 4 (β=0.96)

Fig. 16. Comparison of the effects of pre-stress in chord at ambient temperature and 700 °C, between numerical simulation results and various analytical methods.

Appendix A

Table A.1
Comparison of strength for EHS T and X joints Type 1 (Unit in kN).

Joint name	Simulation results	EN 19931-8 [19] (strength, calculation/simulation ratio)		CIDECT guide No. 3 [23] (strength, calculation/simulation ratio)		Packer et al. [13] (strength, calculation/simulation ratio)	
T90-1C-1	183.8	147.6	0.80	135.8	0.74	156.3	0.85
T90-1C-2	168.2	132.9	0.79	116.5	0.69	141.2	0.84
T90-1C-3	379.0	287.3	0.76	241.5	0.64	297.6	0.79
T90-1C-4	166.4	135.2	0.81	120.9	0.73	145.3	0.87
T90-1C-5	141.2	124.3	0.88	111.9	0.79	134.2	0.95
T90-1C-6	262.1	211.3	0.81	190.0	0.72	226.2	0.86
T90-1C-7	203.4	190.3	0.94	171.8	0.84	205.0	1.01
T90-1C-8	204.5	179.1	0.88	114.6	0.56	194.1	0.95
T30-1C-9	355.7	326.0	0.92	290.5	0.82	347.9	0.98
T45-1C-10	222.6	204.9	0.92	184.3	0.83	219.7	0.99
T60-1C-11	169.2	158.3	0.94	147.8	0.87	168.2	0.99
X90-1C-1	155.5	147.6	0.95	142.9	0.92	132.8	0.85
X90-1C-2	145.3	132.9	0.91	132.3	0.91	119.7	0.82
X90-1C-3	307.0	287.4	0.94	289.1	0.94	258.6	0.84
X90-1C-4	145.3	135.2	0.93	135.2	0.93	121.7	0.84
X90-1C-5	127.6	124.3	0.97	124.3	0.97	111.9	0.88
X90-1C-6	236.4	211.3	0.89	211.2	0.89	190.1	0.80
X90-1C-7	188.5	190.3	1.01	191.1	1.01	171.3	0.91
X90-1C-8	170.1	179.1	1.05	131.4	0.77	161.2	0.95
X30-1C-9	303.1	326.0	1.08	322.8	1.06	293.4	0.97
X45-1C-10	186.1	204.9	1.10	204.7	1.10	184.4	0.99
X60-1C-11	141.8	158.3	1.12	164.2	1.16	142.5	1.00
Average	N/A	N/A	0.93	N/A	0.86	N/A	0.91
Standard deviation	N/A	N/A	10%	N/A	15%	N/A	7%

Table A.2
Comparison of strength for EHS T and X joints Type 2 (Unit in kN).

Joint name	Simulation results	EN 19931-8 [19] (strength, calculation/simulation ratio)		CIDECT guide No. 3 [23] (strength, calculation/simulation ratio)		Packer et al. [13] (strength, calculation/simulation ratio)	
T90-2C-1	230.3	177.8	0.77	157.6	0.68	186.5	0.81
T90-2C-2	196.1	147.0	0.75	130.6	0.67	155.4	0.79
T90-2C-3	551.0	525.3	0.95	460.2	0.84	525.2	0.95
T90-2C-4	199.8	151.2	0.76	134.8	0.67	161.8	0.81
T90-2C-5	159.8	132.5	0.83	118.7	0.74	142.7	0.89
T90-2C-6	311.9	236.3	0.76	210.6	0.68	251.6	0.81
T90-2C-7	228.8	200.9	0.88	184.4	0.81	215.9	0.94
T90-2C-8	222.4	184.9	0.83	164.3	0.74	200.0	0.90
T30-2C-9	396.4	338.6	0.85	302.3	0.76	360.5	0.91
T45-2C-10	238.7	220.3	0.92	204.8	0.86	232.8	0.98
T60-2C-11	187.2	173.2	0.93	166.3	0.89	183.9	0.98
X90-2C-1	190.4	177.8	0.93	177.8	0.93	160.0	0.84
X90-2C-2	171.2	147.0	0.86	147.0	0.86	132.3	0.77
X90-2C-3	474.1	525.3	1.11	541.3	1.14	472.8	1.00
X90-2C-4	175.1	151.2	0.86	151.2	0.86	136.1	0.78
X90-2C-5	118.8	132.5	1.12	132.5	1.12	119.2	1.00
X90-2C-6	279.0	236.3	0.85	236.3	0.85	212.7	0.76
X90-2C-7	214.3	200.9	0.94	202.1	0.94	180.8	0.84
X90-2C-8	167.6	184.9	1.10	184.9	1.10	166.4	0.99
X30-2C-9	314.5	338.6	1.08	335.9	1.07	304.7	0.97
X45-2C-10	213.6	220.3	1.03	220.2	1.03	198.2	0.93
X60-2C-11	175.4	173.2	0.99	173.2	0.99	155.8	0.89
Average	N/A	N/A	0.91	N/A	0.87	N/A	0.89
Standard deviation	N/A	N/A	12%	N/A	15%	N/A	8%

Table A.3
Comparison of strength for EHS T and X joints Type 3 (Unit in kN).

Joint name	Simulation results	EN 19931-8 [19] (strength, calculation/simulation ratio)		CIDECT guide No. 3 [23] (strength, calculation/simulation ratio)		Packer et al. [13] (strength, calculation/simulation ratio)	
T90-3C-1	526.8	280.0	0.53	242.5	0.46	446.0	0.85
T90-3C-2	467.9	209.9	0.45	182.7	0.39	375.4	0.80
T90-3C-3	1005.1	1057.8	1.05	899.1	0.89	968.8	0.96
T90-3C-4	490.0	342.8	0.70	305.1	0.62	395.6	0.81
T90-3C-5	385.4	278.0	0.72	249.1	0.65	330.4	0.86
T90-3C-6	735.3	342.8	0.47	305.6	0.42	623.2	0.85
T90-3C-7	559.5	264.8	0.47	237.9	0.43	497.6	0.89
T90-3C-8	319.7	230.6	0.72	212.0	0.66	292.8	0.92
T30-3C-9	805.5	593.4	0.74	551.8	0.69	750.8	0.93
T45-3C-10	524.3	346.2	0.66	311.6	0.59	508.1	0.97
T60-3C-11	340.0	256.8	0.76	245.0	0.72	325.1	0.96
X90-3C-1	407.7	280.0	0.69	280.0	0.69	351.8	0.86
X90-3C-2	381.1	209.9	0.55	209.9	0.55	315.9	0.83
X90-3C-3	965.1	1057.8	1.10	1057.8	1.10	765.5	0.79
X90-3C-4	380.7	342.8	0.90	342.8	0.90	322.7	0.85
X90-3C-5	345.9	278.0	0.80	278.0	0.80	291.3	0.84
X90-3C-6	601.5	342.8	0.57	342.8	0.57	509.1	0.85
X90-3C-7	519.5	264.8	0.51	264.8	0.51	448.8	0.86
X90-3C-8	308.1	230.6	0.75	230.6	0.75	277.2	0.90
X30-3C-9	640.6	593.4	0.93	593.4	0.93	631.8	0.99
X45-3C-10	495.8	346.2	0.70	346.2	0.70	446.8	0.90
X60-3C-11	389.5	256.8	0.66	256.8	0.66	364.8	0.94
Average	N/A	N/A	0.70	N/A	0.67	N/A	0.88
Standard deviation	N/A	N/A	18%	N/A	18%	N/A	6%

Table A.4
Comparison of strength for EHS T and X joints Type 4 (Unit in kN).

Joint name	Simulation results	EN 19931-8 [19] (strength, calculation/simulation ratio)		CIDECT guide No. 3 [23] (strength, calculation/simulation ratio)		Packer et al. [13] (strength, calculation/simulation ratio)	
T90-4C-2	614.4	568.0	0.92	525.5	0.86	598.8	0.97
T90-4C-5	514.1	459.5	0.89	418.9	0.81	489.2	0.95
T90-4C-7	777.5	390.5	0.50	356.8	0.46	714.2	0.92
T90-4C-8	414.4	277.8	0.67	257.8	0.62	376.6	0.91
T30-4C-9	1255.0	909.5	0.72	845.8	0.67	1197.6	0.95
T45-4C-10	887.4	709.4	0.80	638.5	0.72	846.8	0.95
T60-4C-11	704.5	620.8	0.88	595.0	0.84	691.4	0.98
X90-4C-2	643.0	568.0	0.88	568.0	0.88	533.0	0.83
X90-4C-5	465.0	459.5	0.99	459.5	0.99	397.3	0.85
X90-4C-7	715.7	390.5	0.55	390.5	0.55	580.6	0.81
X90-4C-8	342.1	277.8	0.81	277.8	0.81	314.7	0.92
X30-4C-9	1184.4	909.5	0.77	909.5	0.77	1066.0	0.90
X45-4C-10	817.5	709.4	0.87	709.4	0.87	753.8	0.92
X60-4C-11	653.9	620.8	0.95	620.8	0.95	615.5	0.94
Average	N/A	N/A	0.80	N/A	0.77	N/A	0.91
Standard deviation	N/A	N/A	15%	N/A	15%	N/A	5%

Appendix B. Numerical modelling strategy for EHS T-joints with compensating bending moments

The joint dimension identifier 2 in Table 7 with type 1 orientation of T-joint was used as an example to illustrate modelling the procedure in ABAQUS. A rigid end plate was attached to the chord end as shown in Fig. B.1. The reference point on the rigid plate was used for applying boundary conditions and loads.

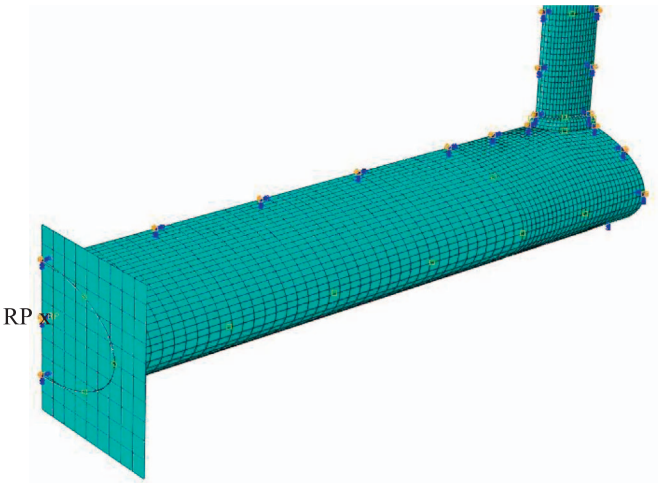

Fig. B.1. Chord end restraints for T90-1C-2.

Two loading steps were implemented in ABAQUS. Fig. B.2 illustrates typical loading conditions of EHS T-joints with chord pre-stress. In order to include the chord pre-stress, the concentrated force (P_1) was applied to the reference point at the end of the chord member in the first step. P_1 can be calculated using Eq. (B.1).

$$P_1 = f_{y0} * A_{chord} * n \tag{B.1}$$

Assume the chord pre-stress ratio to be (n =) − 0.4. The cross sectional area of the chord member was 45.1 cm^2. Hence, the concentrated load (P_1) was 640.4 kN.

In the second loading step, an axial load in the brace (P_2) and compensating bending moments ($M_{0,chord}$) at the chord ends were applied together. The magnitude of the compensating bending moments ($M_{0,chord}$) is equal but opposite to the maximum bending moment in the chord generated by the axial force P_2 in the brace, as calculated as follows:

$$M_{0,chord} = \frac{P_2(L-d)}{4} \tag{B.2}$$

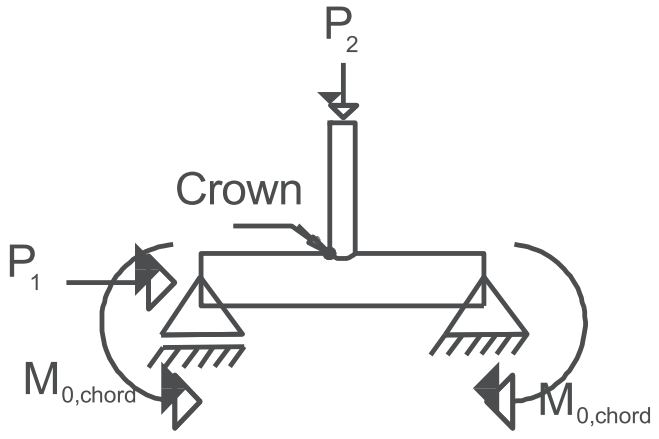

Fig. B.2. Typical loading condition for EHS T-joints with chord pre-stress.

Appendix C

Table C.1
Comparison of strengths for EHS T and X joints with n = 0.0 or −0.4 at ambient temperature, between numerical simulation results and various analytical methods (Unit in kN).

Joint name	CIDECT guide No. 3 [23]			EN 19931-8 [19]			Packer et al. [13]			Simulation results		
	n = 0	n = −0.4	$\frac{n=-0.4}{n=0}$	n = 0	n = −0.4	$\frac{n=-0.4}{n=0}$	n = 0	n = −0.4	$\frac{n=-0.4}{n=0}$	n = 0	n = −0.4	$\frac{n=-0.4}{n=0}$
T90-1C-2	132.9	103.7	0.78	132.9	84.2	0.63	146.2	131.5	0.95	173.2	161.3	0.93
X90-1C-2	132.9	103.7	0.78	132.9	84.2	0.63	104.8	94.3	0.90	145.3	138.5	0.95
T90-2C-2	147.0	122.0	0.83	147.0	142.6	0.97	161.7	145.5	0.90	205.9	189.4	0.92

X90-2C-2	147.0	122.0	0.83	147.0	142.6	0.97	132.3	119.1	0.90	171.2	162.6	0.95
T90-3C-2	209.9	174.2	0.83	209.9	203.6	0.97	380.3	342.3	0.90	470.0	437.8	0.93
X90-3C-2	209.9	174.2	0.83	209.9	203.6	0.97	377.4	339.6	0.90	381.1	366.0	0.96
T90-4C-2	568.0	539.6	0.95	568.0	568.0	1.00	609.7	548.8	0.90	620.5	595.7	0.96
X90-4C-2	568.0	539.6	0.95	568.0	568.0	1.00	636.7	573.0	0.90	643.0	610.8	0.95

Table C.2
Comparison of strengths for EHS T and X joints with n = 0.0 or −0.4 at 700 °C, between numerical simulation results and various analytical methods (Unit in kN).

Joint name	CIDECT guide No. 3 [23]			EN 19931-8 [19]			Packer et al. [13]			Simulation results			
	n = 0	n = −0.4	$\frac{n=-0.4}{n=0}$	n = 0	n = −0.4	$\frac{n=-0.4}{n=0}$	n = 0	n = −0.4	$\frac{n=-0.4}{n=0}$	n = 0	n = −0.4	$\frac{n=-0.4}{n=0}$	$\frac{n=-0.4}{n=0}$
T90-1C-2	30.6	23.9	0.78	30.6	19.4	0.63	33.6	30.2	0.95	27.7	24.9	0.90	
X90-1C-2	30.6	23.9	0.78	30.6	19.4	0.63	24.1	21.7	0.95	24.7	22.7	0.92	
T90-2C-2	33.8	28.1	0.83	33.8	32.8	0.97	37.2	33.5	0.90	33.0	30.0	0.91	
X90-2C-2	33.8	28.1	0.83	33.8	32.8	0.97	30.4	27.4	0.90	25.7	23.9	0.93	
T90-3C-2	48.3	40.1	0.83	48.3	46.8	0.97	87.5	78.7	0.90	98.7	90.0	0.91	
X90-3C-2	48.3	40.1	0.83	48.3	46.8	0.97	86.8	78.1	0.90	83.8	78.8	0.94	
T90-4C-2	130.6	124.1	0.95	130.6	130.6	1.00	140.2	126.2	0.90	136.2	127.0	0.93	
X90-4C-2	130.6	124.1	0.95	130.6	130.6	1.00	146.4	131.8	0.90	141.5	131.6	0.93	

References

[1] Chan T, Gardner L. Flexural buckling of elliptical hollow section columns. J Struct Eng 2009;135:546–57.
[2] Ruiz-Teran A, Gardner L. Elastic buckling of elliptical tubes. Thin-Walled Struct 2008;46:1304–18.
[3] Narendra PV, Singh KD. Elliptical hollow section steel cantilever beams under extremely low cycle fatigue flexural load–a finite element study. Thin-Walled Struct 2017;119:126–50.
[4] Ozyurt E, Wang YC, Tan KH. Elevated temperature resistance of welded tubular joints under axial load in the brace member. Eng Struct 2014;59:574–86.
[5] Bortolotti E, Jaspart JP, Pietrapertosa C, Nicaud G, Petitjean P, Grimault JP. Testing and modelling of welded joints between elliptical hollow sections. Proc. 10th Int. Symp. on Tubul. Struct. 2003. p. 259–66.
[6] Pietrapertosa C, Jaspart JP. Study of the behaviour of welded joints between elliptical hollow sections. Proc. 10th Int. Symp. Tubul. Struct. 2003. p. 601–8.
[7] Choo YS, Liang JX, Lim LV. Static strength of elliptical hollow section X-joint under brace compression. Proc. 10th Int. Symp. Tubul. Struct. 2003. p. 253–8.
[8] Shen W, Choo YS, Wardenier J, Packer JA, Van Der Vegte GJ. Static strength of axially loaded EHS X-joints with braces welded to the narrow sides of the chord. J Constr Steel Res 2013;88:181–90.
[9] Shen W, Choo YS, Wardenier J, Packer JA, Van Der Vegte GJ. Static strength of axially loaded elliptical hollow section X joints with braces welded to wide sides of chord. I: numerical investigations based on experimental tests. J Struct Eng 2014;140:4013035.
[10] Shen W, Choo YS, Wardenier J, Van Der Vegte GJ, Packer JA. Axially loaded elliptical hollow section X joints, part I: experiments and numerical calibration. Proc. 14th Int. Symp. Tubul. Struct. London, UK: CRC Press; 2012. p. 257–64.
[11] Shen W, Wardenier J, Packer JA, Choo YS, Van Der Vegte GJ. Axially loaded elliptical hollow section X joints, part II: results and analysis. Proc. 14th Int. Symp. Tubul. Struct. London, UK: CRC Press; 2012. p. 265–72.
[12] Wardenier J, Choo YS, Packer JA, Van der Vegte GJ, Shen W. Design recommendations for axially loaded elliptical hollow section X and T joints. Steel Constr 2014;7:89–96.
[13] Packer JA, Choo YS, Shen W, Wardenier J, Van der Vegte GJ, Mustard T. Axially loaded T and X joints of elliptical hollow sections. Final Rep 5BW-2. CIDECT; 2012.
[14] Haque T, Packer JA. Elliptical hollow section T and X connections. Can J Civ Eng 2012;39:925–36.
[16] Shao Y, Zheng Y, Zhao H, Yang D. Performance of tubular T-joints at elevated temperature by considering effect of chord compressive stress. Thin-Walled Struct 2016;98:533–46.
[17] Feng R, Young B. Design of cold-formed stainless steel tubular joints at elevated temperatures. Eng Struct 2012;35:188–202.
[18] Nguyen MP, Tan KH, Fung TC. Numerical models and parametric study on ultimate strength of CHS T-joints subjected to brace axial compression under fire condition. Proc. 13th int. symp. tubul. struct., Hong Kong, China. 2010. p. 733–40.
[19] BS EN 1993-1-8. Eurocode 3: design of steel structures - part 1–8: design of joints. Brussels, Belgium: European Commitee for Standardization (CEN); 2005.
[20] Wardenier J, Kurobane Y, Packer JA, Van der Vegte GJ, Zhao XL. Design guide for Circular Hollow Section (CHS) joints under predominantly static loading. CIDECT. TUV Rheinland; 2008.
[21] Shen W, Choo YS, Wardenier J, Packer JA, Van Der Vegte GJ. Static strength of axially loaded elliptical hollow section X joints with braces welded to wide sides of chord. II: parametric study and strength equations. J Struct Eng 2012;140:4013036.
[22] Haque T, Packer JA, Zhao XL. Equivalent RHS approach for the design of EHS in axial compression or bending. Adv Struct Eng 2012;15:107–20.
[23] Packer JA. Design guide for Rectangular Hollow Section (RHS) joints under predominantly static loading. CIDECT. Verlag TUV Rheinland; 1992.
[24] Packer JA, Wardenier J, Choo YS, Chiew SP. Elliptical steel tubes. Steel news notes, Singapore struct. steel soc. SN&N 25th anniv. issue. 2009. p. 86–90.
[25] Zhao XL, Kernot A, Packer JA, Haque T. Slenderness limits for EHS and OHS subject to bending using the RHS approach. Proc. 13th int. symp. tubul. struct. Hong Kong, China. 2010. p. 293–302.
[26] Lan X, Huang Y. Structural design of cold-formed stainless steel tubular X-and T-joints at elevated temperatures. Thin-Walled Struct 2016;108:270–9.
[27] He S, Shao Y, Zhang H. Evaluation on fire resistance of tubular K-joints based on critical temperature method. J Constr Steel Res 2015;115:398–406.
[28] Tan KH, Fung TC, Nguyen MP. Structural behavior of CHS T-joints subjected to brace axial compression in fire conditions. J Struct Eng 2013;139:73–84.
[29] Lan X, Wang F, Luo Z, Liu D, Ning C, Xu X. Joint strength reduction factor of internally ring-stiffened tubular joints at elevated temperatures. Adv Struct Eng 2016;19:1650–60.
[30] Abaqus V. 6.14-1. Abaqus/standard user's manual and Abaqus CAE manual. Providence, RI, USA: Dassault Systemes Simulia Corp.; 2014.
[31] Ozyurt E, Wang YC. Effects of truss behaviour on critical temperatures of welded steel tubular truss members exposed to uniform fire. Eng Struct 2015;88:225–40.
[32] Boresi AP, Schmidt RJ. Advanced mechanics of materials. 6th ed. John Wiley and Sons; 2009.
[33] Lu LH, De Winkel GD, Yu Y, Wardenier J. Deformation limit for the ultimate strength of hollow section joints. Proc. 6th Int. Symp. Tubul. Struct. 1994. p. 341–7.
[34] He S, Shao Y, Zhang H, Wang Q. Parametric study on performance of circular tubular K-joints at elevated temperature. Fire Saf J 2015;71:174–86.
[35] Cheng C, Yongbo S, Jie Y. Experimental and numerical study on fire resistance of circular tubular T-joints. J Constr Steel Res 2013;85:24–39.
[36] BS EN 1993-1-2. Eurocode 3: design of steel structures - part 1–2: structural fire design. Brussels, Belgium: European Commitee for Standardization (CEN); 2005.